Journal of Spacecraft and Rockets
Vol. 52, No. 2, March–April 2015

Interplanetary Dust Particle Shielding Capability of Spacecraft Multilayer Insulation

Kaushik A. Iyer* and Douglas S. Mehoke†
Johns Hopkins Applied Physics Laboratory, Laurel, Maryland 20723
and
Romesh C. Batra‡
Virginia Polytechnic Institute and State University, Blacksburg, Virginia 24061

DOI: 10.2514/1.A33101

Definition of interplanetary dust particle hypervelocity impact protection levels provided by spacecraft multilayer insulation/thermal blankets is provided for the first time. Development of a new data-anchored shock-hydrocode-computations-derived ballistic limit equation in the 7–150 km/s hypervelocity impact range for representative two-wall Whipple shields, in which spacecraft multilayer insulation is the bumper material impacted by fused silica dust, is presented. A baseline configuration was adopted for analysis: 0.0176-cm-thick Kapton bumper (monolithic and layered), 2.54 cm standoff, and 0.0762-cm-thick titanium alloy Ti-6Al-4V rear wall. Significant efforts made to verify and validate the computational methodology with hypervelocity impact test data are also described. With a solid Kapton bumper, the critical particle diameter for causing incipient spall in the rear wall, which is chosen to be the failure criterion, is found to be in the ~650–1100 μm range, with the largest and the smallest sizes corresponding to 30 and 150 km/s hypervelocity impact, respectively. When the bumper is layered in a manner similar to that found in actual blankets (140 μm spacing), the critical particle diameter is indicated to be in the ~450–600 μm range.

Downloaded by VIRGINIA TECHNICAL UNIVERSITY on March 18, 2015 | http://arc.aiaa.org | DOI: 10.2514/1.A33101

I. Introduction

THE Solar Probe Plus (SPP) spacecraft will rely on thermal blankets/multilayer insulation (MLI) to function additionally as shielding against interplanetary dust particle (IDP) hypervelocity impacts (HVIs) during its approximately seven year journey to achieve a final mission orbit with a perihelion distance of less than 10 solar radii. Mission assurance necessitates definition of IDP HVI protection levels provided by the spacecraft's MLI with a reliability that is similar to that available for metallic Whipple shields for the first time. The predicted cumulative dust flux profile for SPP is similar to those obtained for other recent interplanetary spacecraft such as Mars Reconnaissance Orbiter (MRO), Cassini to Saturn and its moons (Cassini), New Horizons (NH) to Pluto, Juno to Jupiter, and SPP is shown in Fig. 1. The main difference for the SPP dust HVI mitigation is the extreme speed of impacts that warrant consideration (i.e., up to 150 km/s). The SPP dust study is using the experience from those programs, supplemented with new necessary testing and a new analytical capability that extends the velocity range.

The MLI in SPP will generally be in two-wall Whipple shield configurations [1], in which the blanket is the bumper shield and a spacecraft structural surface or other functional component is the rear wall. The MLI will be directly exposed to the dust flux (Fig. 2). MLI has generally been used as internal "stuffing" [1,2] between the bumper and rear wall, as well as the bumper (e.g., for the Soyuz orbital module), when augmented with perforated aluminum alloy plates and fiberglass [3]. Owing to the extreme impact speeds involved in SPP design, rear wall damage predictions from hypervelocity blast loading of hot, vaporized dust and MLI blanket materials is needed; this is different from much of the focus of the existing body of spacecraft micrometeoroid and orbital debris (MMOD) shielding work, which is on microscale particulate debris clouds generated at ~7–10 km/s [1,4].

Owing to the range of shielding configurations that warrant consideration (different blanket layering/areal densities, standoff distances, and rear wall materials and thicknesses), an analytical equation, that is, ballistic limit equation (BLE) [1,3], is desired for generalizing particular results and quantitatively specifying design requirements for SPP blankets.

This paper presents a multiphysics shock-hydrocode-computations-based approach that combines impact shock physics analyses, high-rate material thermodynamic and strength response models, verified and validated shock hydrocode computations, and HVI test data with design considerations, described previously for monolithic shielding materials and layered solids such as solar arrays [5,6], to explicitly address the range of Whipple shield debris/vapor cloud phases specific to the extreme SPP impact speeds and develop a broadly applicable BLE for normal (nonoblique) impacts.

II. Whipple Shield BLE and Shielding Mechanisms

Figure 3 depicts an existing well-known two-wall Whipple shield BLE for normal impacts [1]. In broad terms, the BLE is in fact a connected set of three different equations, each valid over a specific impact speed range (<3, 3–7, and >7 km/s), which in turn correspond to three different dust/particle response modes following impact with the bumper shield but before impact with the rear wall (ballistic deformation, fragmentation and partial melt, and melt/vaporization). The set of equations that comprise this BLE are:

$$d_c = \left[\frac{t_b + \sqrt{\sigma/40} \cdot t_w}{0.6\sqrt{\rho_p} V^{2/3} (\cos\theta)^{5/3}}\right]^{18/19} \tag{1}$$

when the normal component of the impact velocity, $V\cos\theta$, is ≤ 3 km/s,

Received 3 July 2014; revision received 23 September 2014; accepted for publication 6 October 2014; published online 5 January 2015. Copyright © 2014 by the American Institute of Aeronautics and Astronautics, Inc. Under the copyright claimed herein, the U.S. Government has a royalty-free license to exercise all rights for Governmental purposes. All other rights are reserved by the copyright owner. Copies of this paper may be made for personal or internal use, on condition that the copier pay the $10.00 per-copy fee to the Copyright Clearance Center, Inc., 222 Rosewood Drive, Danvers, MA 01923; include the code 1533-6794/15 and $10.00 in correspondence with the CCC.

*Materials Physicist and Section Supervisor, Space Department, 11100 Johns Hopkins Road, Mail Stop 200-E345.
†Assistant Technology Manager and Group Supervisor, Space Department, 11100 Johns Hopkins Road, Mail Stop 23-380.
‡Clifton C. Garvin Professor, Department of Biomedical Engineering and Mechanics, M/C 0219.

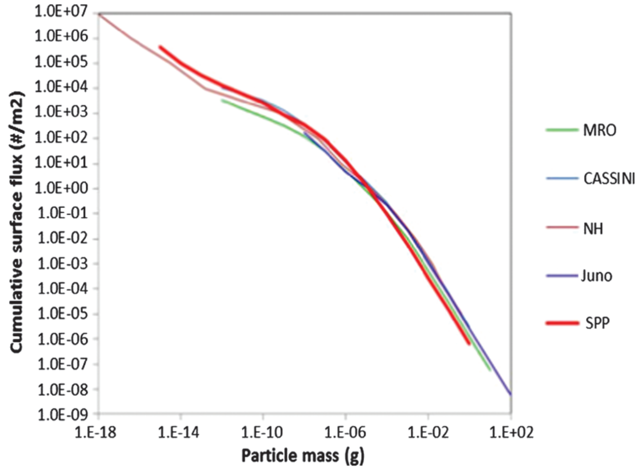

Fig. 1 Predicted dust environment for SPP compared with other recent interplanetary missions.

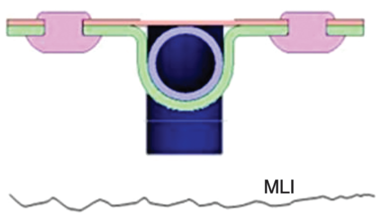

Fig. 2 Representative two-wall Whipple shield configuration in SPP in which the bumper will be a thermal blanket/MLI.

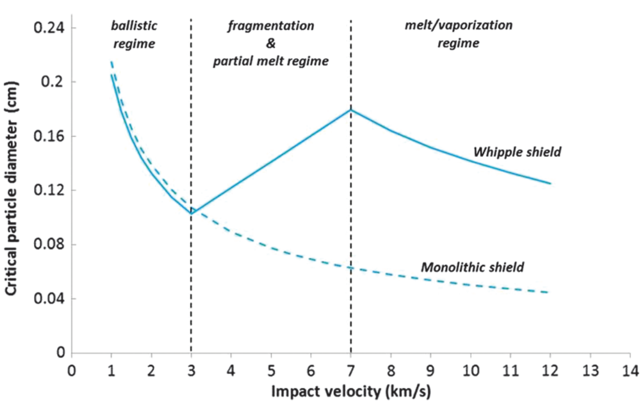

Fig. 3 Representation of the enhancement in shielding performance obtained with a two-wall Whipple shield configuration that has the same mass (combined thickness) as a monolithic shield [1].

$$d_c = \left[1.75 - \frac{V\cos\theta}{4}\right]\left[\frac{t_b + \sqrt{\sigma/40}\cdot t_w}{1.248\sqrt{\rho_p}\cos\theta}\right]^{18/19} + \left[\frac{V\cos\theta}{4} - 0.75\right]\left[1.071 t_w^{2/3}\rho_p^{-1/3}\rho_b^{-1/9}S^{1/3}(\sigma/70)^{1/3}\right] \quad (2)$$

when the normal component of the impact velocity is 3–7 km/s, and

$$d_c = 3.918 t_w^{2/3}\rho_p^{-1/3}\rho_b^{-1/9}S^{1/3}(\sigma/70)^{1/3}(V\cos\theta)^{-2/3} \quad (3)$$

when the normal component of the impact velocity is $>$ 7 km/s; and where d_c (cm) is the critical particle diameter for inducing failure of the rear (spacecraft) wall, ρ_p(g/cc) is the particle density, ρ_b(g/cc) is the bumper density, t_w (cm) is the rear wall thickness, S (cm) is the standoff of the rear wall from the bumper, σ (ksi) is the rear wall yield stress, V is the particle impact velocity, and θ is the impact angle relative to the normal direction such that $V\cos\theta$ is the normal component of the impact velocity.

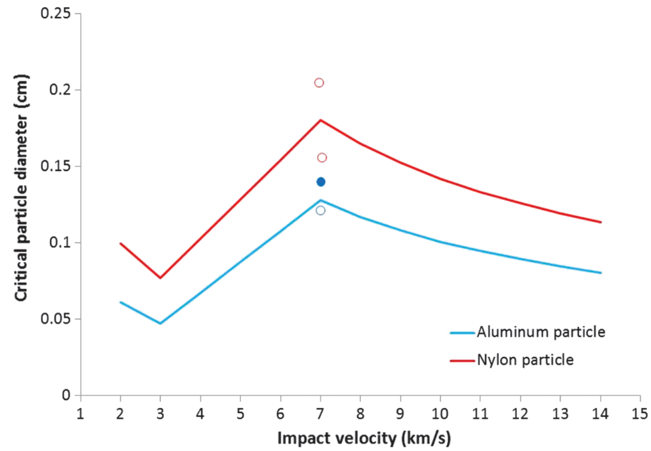

Fig. 4 Comparison of measured and BLE-predicted performance of a two-wall Whipple configuration.

Ultimately, the BLE shown is used to predict the smallest solid spherical particle that will cause failure of the rear wall at a given impact (normal) speed (i.e., the critical particle size) for a two-wall configuration specified by a bumper material and thickness, standoff, and rear wall material and thickness. Historically, BLEs have been constructed and applied with the aid of test data, engineering expertise, and selective hydrocode computations [1,2]. Also, available two-wall Whipple shield BLEs have mostly been developed for configurations with metallic (generally aluminum alloy) bumpers and with data in the 3–8 km/s HVI range. The BLEs shown in Fig. 3 are based on a 0.06 cm-thick aluminum alloy bumper, 1.5 cm standoff, 0.15-cm-thick aluminum rear wall, and an aluminum alloy particle.

III. Available Whipple Shield BLEs for Solar Probe

For SPP, a BLE that treats MLI as the bumper material and accounts for dust HVI response that may be entirely in the vaporization regime is required. One way to address the first aspect (i.e., MLI bumper instead of metallic bumper) is to simply interpret the existing BLE in terms of areal density (MLI blankets are specified by their areal density, whereas metallic/monolithic bumpers are specified by their volumetric density) and use an aluminum alloy monolithic bumper with the same areal density as the MLI.

Figure 4 shows the efficacy of using this approach for a two-wall Whipple shield configuration in which a 0.076 g/cm^2 MLI is the bumper 3.81 cm standoff, and an aluminum alloy honeycomb structure is the rear wall (open symbols denote pass and closed symbols denote fail). The MLI includes an innermost layer of 0.025 g/cm^2 beta-cloth (facing the honeycomb). The honeycomb wall consists of a 1.27-cm-thick aluminum honeycomb core with 0.0254-cm-thick aluminum alloys face sheets on front and back side of core.

The points are test data and the curves are BLEs obtained by treating the MLI as an aluminum plate with the same areal density and the rear wall as a monolithic aluminum plate with a thickness equal to that of the honeycomb front and back faces combined. As the comparisons show, this approach correctly predicts the critical aluminum particle diameter. However, the predicted critical nylon particle diameter at 7 km/s is noticeably smaller than the actual size, which was not determined. From the design standpoint, both outcomes are useful because they are either accurate or conservative. With the aluminum particle, it is believed that approximating the MLI as aluminum alloy monolith with the same areal density over-represents the bumper's shielding capacity and that approximating the honeycomb structure as a monolith underrepresents the rear wall's shielding capacity, and that these two effects cancel each other sufficiently leading to a fortuitously accurate prediction.

Figure 5 shows the accuracy of using this approach for another two-wall Whipple shield configuration in which a 0.162 g/cm^2 MLI is the bumper, consisting of a 0.162 g/cm^2 MLI bumper, 10.16 cm

Downloaded by VIRGINIA TECHNICAL UNIVERSITY on March 18, 2015 | http://arc.aiaa.org | DOI: 10.2514/1.A33101

Downloaded by VIRGINIA TECHNICAL UNIVERSITY on March 18, 2015 | http://arc.aiaa.org | DOI: 10.2514/1.A33101

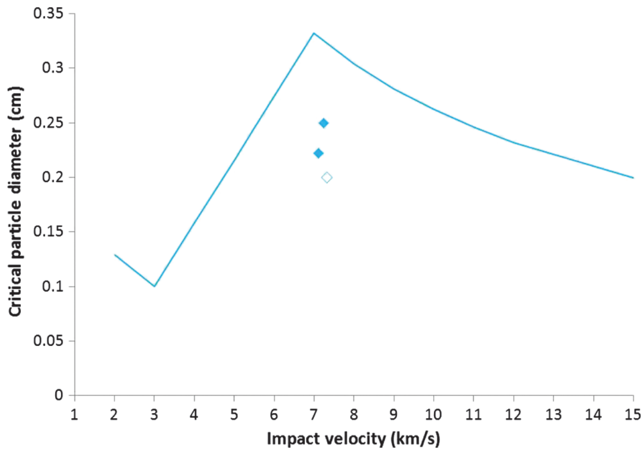

Fig. 5 Comparison of measured and BLE-predicted performance of a two-wall Whipple configuration.

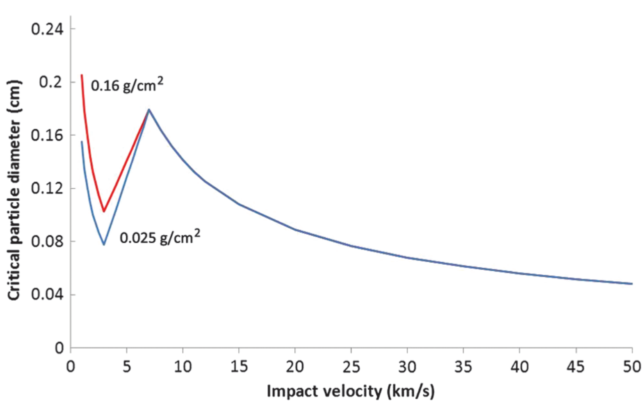

Fig. 6 Illustrative two-wall Whipple shield BLE showing the effect of changing the bumper areal density on the predicted critical particle size.

standoff, and a 0.0813-cm-thick Ti-6Al-4V titanium alloy rear wall. The MLI includes an innermost layer of Kevlar. Comparison of the BLE with the HVI test data shows that the BLE is not conservative in this case and overestimates the protection level by a factor of ~1.5×.

In addition to the absence of a reliable correlation between the existing two-wall Whipple shield BLE and test data, some of the trends predicted by the BLE in the high-velocity regime (7 km/s and higher) do not appear realistic. Figure 6 illustrates that the approach of replacing an MLI bumper with an aluminum bumper with the same areal density for predicting critical particle diameters is insensitive to the MLI thickness/areal density above 7 km/s. Further, the existing BLE predicts greater protection for a less dense bumper material, which contradicts data. These considerations lead one to conclude that the shock-driven materials phase changes and vapor blast-induced structural damage physics up to 300 km/s must be addressed more directly for gaining a reliable Whipple shield performance predictive capability.

The need for reliable physics-based prediction of MLI dust shielding capability up to 300 km/s is essential for SPP and is the driver for the present work. This paper describes development of a two-wall Whipple shield BLE in which MLI is the bumper and the dust material is fused silica, for application to various SPP spacecraft surfaces and components. The process followed accounts for several major modeling/design decision-related aspects, including treatment of Whipple shield HVI physics in the dust/bumper vaporization regime, verification and validation of computational analyses at impact speeds higher than previously considered, treatment of layered versus monolithic bumpers, treatment of MLI layer spacing, addressing numerical problems at impact speeds below 30 km/s using three-dimensional (3-D) computations, and maximizing the use of limited available test data for Whipple shields with MLI as a bumper. Each of these aspects and the newly developed BLE are described in the subsequent sections.

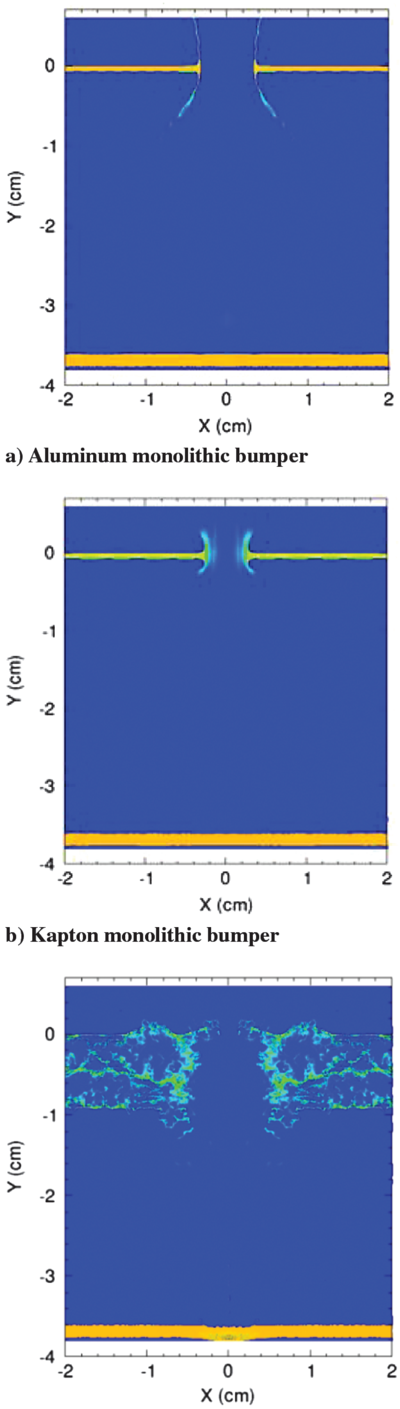

a) Aluminum monolithic bumper

b) Kapton monolithic bumper

c) MLI

Fig. 7 The two-wall Whipple shield configuration used for verification of the computations.

IV. Treatment of HVI Whipple Shield Physics

Following the advancement of the Whipple shield concept [7] as a lightweight solution to MMOD shielding, the underlying physics received significant attention in subsequent years. Maiden et al. [8], Madden [9], Nysmith [10], Richardson [11], and others developed theoretical energy and/or momentum conservation equations along with geometric considerations and assumption of debris dispersion and idealized rear wall mechanical failure criteria as a means of understanding and predicting the failure (ballistic limit) of two-wall metallic configurations. The works by Maiden et al. [8] and Madden [9] are particularly relevant to SPP because their analyses addressed hypervelocity vapor clouds striking a rear wall rather than solid and molten particulate debris [1,12]. Hopkins et al. [13] and Schmidt et al. [14] extended these previously developed ballistic limit approaches through additional analyses and direct experiments with cadmium and flash x-ray visualization because melting and vaporization can be induced in this material at ground HVI speeds (3–10 km/s); Maiden et al. [8] had also performed some tests with cadmium. The experiments by Schmidt et al. [14] provide unique detailed data on the performance of two-wall shields under particle impact vaporization conditions and are used in the present work for validating the hydrocode computations.

To overcome the limitations of the theoretical analyses (e.g., vapor/debris cloud shock induced cratering and spall failure in the rear wall cannot be easily analyzed), direct numerical simulation of HVI of Whipple shields using shock hydrocodes have also been performed [1,4,15–18]. Christiansen et al. [1] report use of the CALE hydrocode to compute the fraction of projectile material in the debris cloud as a function of bumper thickness to particle diameter ratio in the 6–14 km/s impact speed range. The study reported that only 5–6% of the projectile melted at 6 km/s regardless of bumper thickness, and 99% of the projectile melted following a 14 km/s impact into a bumper that is one-fifth as thick as the projectile diameter. Chhabildas et al. [4] used the CTH [19] hydrocode to perform detailed two-dimensional (2-D) (axisymmetric) simulations of HVI tests involving a prototypical two-wall Whipple shield configuration for MMOD studies (aluminum alloy projectile, bumper, and rear wall) at about 10 km/s. They found that the hydrocode simulation adequately predicted the performance (pass or failure) of the Whipple shield but predicted peak axial and lateral debris cloud speeds that were less than the measured values. They attribute the difference to a limitation with the equation of state (EOS) used for aluminum alloy 6061-T6. Subsequently, Hertel et al. [16] performed a detailed comparison of measured and computed debris cloud characteristics generated by HVI of zinc spheres on thin zinc plates and verified that the CTH hydrocode can accurately predict debris structure and subsequent momentum transfer to the rear wall in a Whipple shield, subject to availability of accurate EOS and material strength and damage models. For the present work, the CTH hydrocode was used.

V. Extension of Whipple Shield Damage Computations up to 150 Kilometers per Second

Although the CTH hydrocode has been verified for its capability for performing Whipple shield damage calculations up to ∼10 km/s [4,16], additional verification was sought because the majority of the anticipated dust impacts for SPP design are in the 15–150 km/s range, and hydrocodes are not known to have been used previously for these extreme impact speeds. Further, verification of the capability for modeling the Kapton layers in MLI was also desired. To this end, a first series of computations was performed with a two-wall configuration similar to that tested recently by Piekutowski et al. [2] above 9 km/s, over the range of impact speeds and bumper materials and configurations relevant to SPP. These computations were performed to ensure that CTH has the capacity to define the development and hypervelocity expansion of hot nonuniform particulate and vapor clouds, with low to very low density resulting from HVI of a microscale dust particle with a bumper, and to transfer the shock energy and momentum from this cloud to the rear wall and define the development of relevant failure modes such as incipient spall, detached spall, and perforation. The computations were 2-D (axisymmetric) and considered aluminum and fused silica particles, aluminum monolithic, Kapton monolithic, and Kapton layered bumpers, and impacts in the range of 4–150 km/s (Fig. 7).

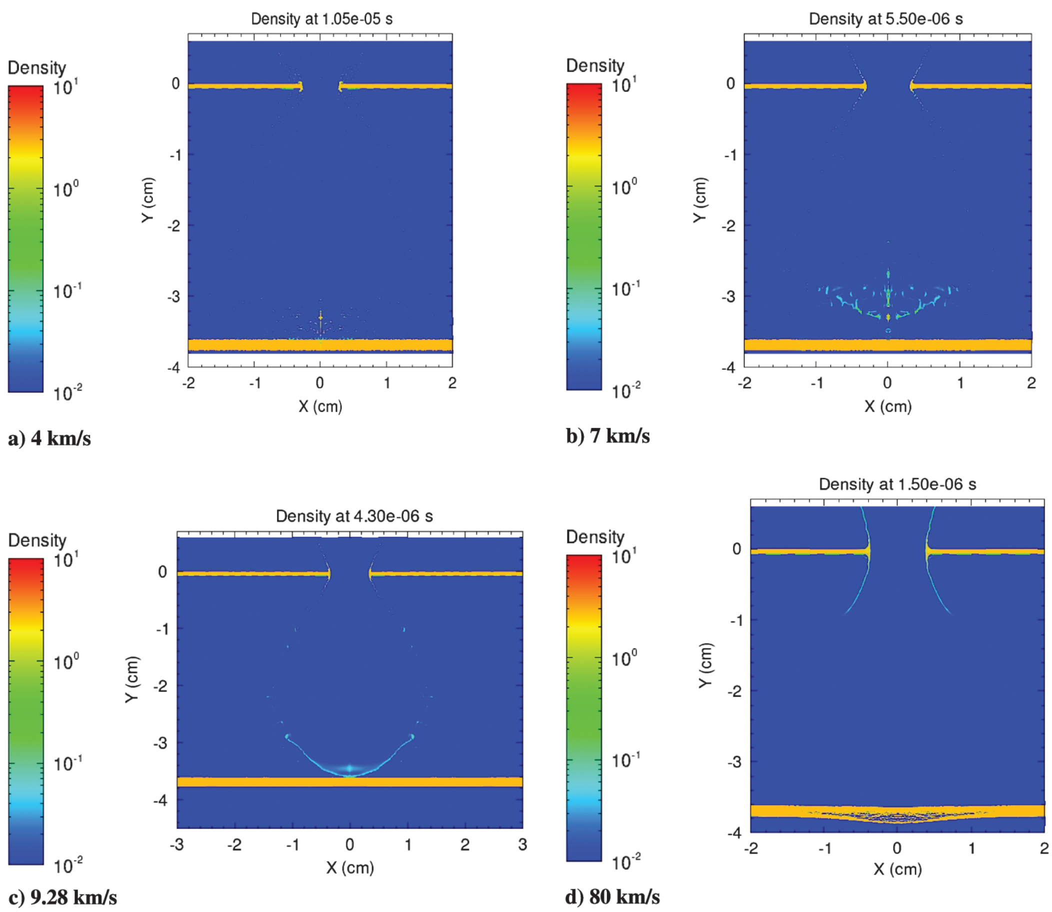

Fig. 8 Particulate and vapor clouds striking the rear wall for four impact speeds.

Downloaded by VIRGINIA TECHNICAL UNIVERSITY on March 18, 2015 | http://arc.aiaa.org | DOI: 10.2514/1.A33101

Downloaded by VIRGINIA TECHNICAL UNIVERSITY on March 18, 2015 | http://arc.aiaa.org | DOI: 10.2514/1.A33101

The Kapton monolithic and MLI-like bumpers used in these verification computations had the same areal density as a 0.0635-cm-thick aluminum alloy bumper. The MLI-like bumper had finely spaced, microthin Kapton layers as follows: one outer 80-μm-thick layer of Kapton, 19 layers of 25-μm-thick Kapton separated by 420 μm, and one inner 80-μm-thick layer of Kapton. This layering configuration was developed by scaling an actual MLI stackup [20] by ~3× to obtain the required areal density.

Adaptive mesh refinement with square cells as small as 12.5×12.5 μm was eventually used for this first series of calculations. This level of resolution was determined to be more than adequate following consideration of the need for adequate resolution of the rear wall and bumper in the through-thickness directions [4,16] and accuracy in reproducing images of particulate debris clouds obtained at 6.64 km/s using flash radiography [12], as well as prior experience in developing grids suitable for obtaining excellent predictions of incipient spall in relatively thick titanium alloy shielding plates [21]. As presented in the validation analyses that follow, adequacy of mesh resolutions used were ultimately determined by the capability to predict rear wall failure modes observed in experiments. An analytical EOS was used for Kapton, and tabular equations of state were used for the remaining materials [22,23]. Johnson–Cook strength and failure models, along with spall strength values, were used for the aluminum alloy bumper, rear wall, and particle [21,22]. No strength model was used for fused silica and Kapton because these are considered to be of negligible importance at the impact speeds and shock pressures of interest (i.e., the response of the bumpers and small dust particles at the extreme impact speeds of interest will be determined primarily by the shock-induced phase changes governed by their respective equations of state, and the opportunity for the development of low hydrostatic pressure or strength-relevant states is limited owing to relatively small through-thicknesses or diameters).

Figure 8 shows plots of the debris/vapor cloud that develops as impact speed increases with an aluminum alloy particle and bumper. Consistent with expectations, the computations show that the content of the cloud striking the rear wall changes from fine solid and molten particulates predominantly at lower speeds and shock pressures (Figs. 8a and 8b) to relatively dense vapor at higher speeds (Fig. 8c) or highly rarified vapor at very high speeds and shock pressures (Fig. 8d). A clustering of particulate material along the symmetry axis ($x = 0$) is noted at the lower speeds, whereas this feature does not develop when the cloud content is entirely vaporized material. The 3-D computations described later show this feature to a lesser extent.

Figure 9 shows the incipient spall developed in the rear wall for a range of representative impact speeds. The computations are found to be capable of predicting incipient spall development with the requisite degree of sensitivity. At 15 km/s HVI (Fig. 9a), the rear wall exhibits notable bending, also demonstrating that the computations are capable of representing the larger scale rear wall structural deformation. Particular care was given to ensuring adequate grid resolution for capturing shock propagation in the rear wall. Separate adaptive mesh refinement in the rear wall was used (Fig. 9d) because additional local resolution was found to be required to track the pressure front and damage evolution. All computations were run until complete shock release in the rear wall was achieved.

Figure 10, which summarizes some of the results of the verification computations performed, shows that the computations correctly predict a reduction in critical particle diameter when Kapton is used instead of aluminum for the bumper. Critical diameters are shown for an aluminum alloy monolithic or a Kapton monolithic bumper. For the configuration examined, a diminishing reduction in critical particle diameter is indicated as the impact speed increases. For comparison purposes, the two corresponding BLEs were also evaluated. The level of protection achieved is indicated to be 1.5–2 times greater than that predicted by the BLEs. It is noted that the computed BLE with an aluminum bumper is indicated to be steeper than that with a Kapton bumper.

Some computations were also performed to obtain an assessment of the influence of spacing between the layers and dust material. Rather than an aluminum alloy, fused silica [23] is a more appropriate representation of the dust material that SPP is expected to encounter. Figure 11 shows that the two-wall Whipple shield computations are

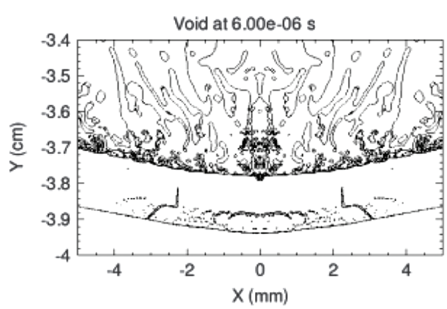

a) 0.28-cm-diam at 15 km/s

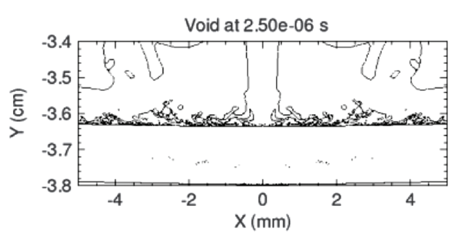

b) 0.18-cm-diam at 50 km/s

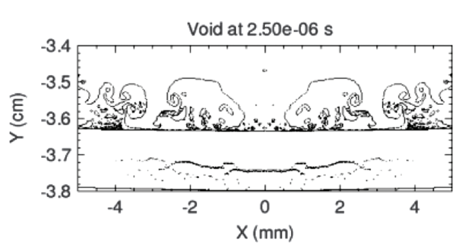

c) 0.15-cm-diam at 80 km/s

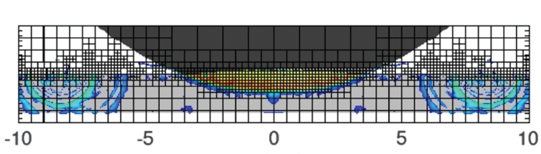

d) Adaptive mesh refinement of rear wall

Fig. 9 Incipient spall development in the rear wall of the all-aluminum two-wall Whipple shield configuration described in Fig. 7 following impact by an aluminum alloy particle.

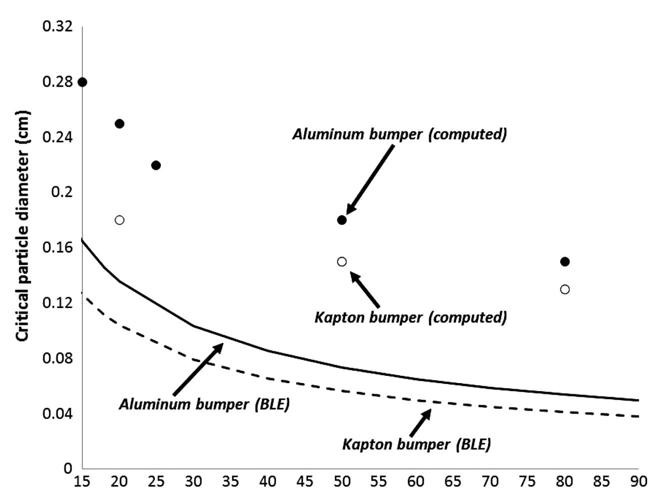

Fig. 10 Computationally determined critical particle diameter for causing incipient spall in the rear wall of the two-wall Whipple shield configuration described in Fig. 7 in the 15–80 km/s HVI range.

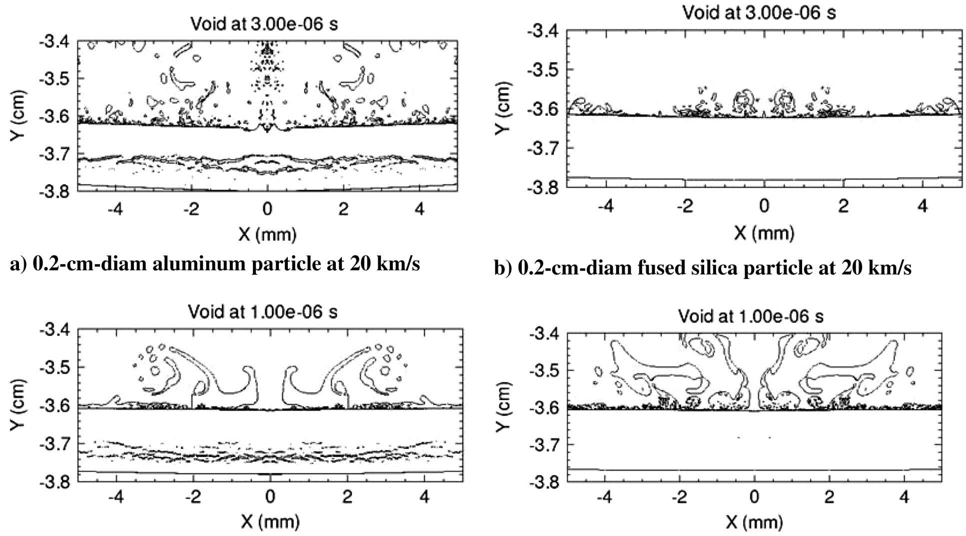

a) 0.2-cm-diam aluminum particle at 20 km/s

b) 0.2-cm-diam fused silica particle at 20 km/s

c) 0.14-cm-diam aluminum particle at 80 km/s

d) 0.14-cm-diam fused silica particle at 80 km/s

Fig. 11 Effect of dust material on incipient spall development in the configuration described in Fig. 7 with a Kapton monolithic bumper.

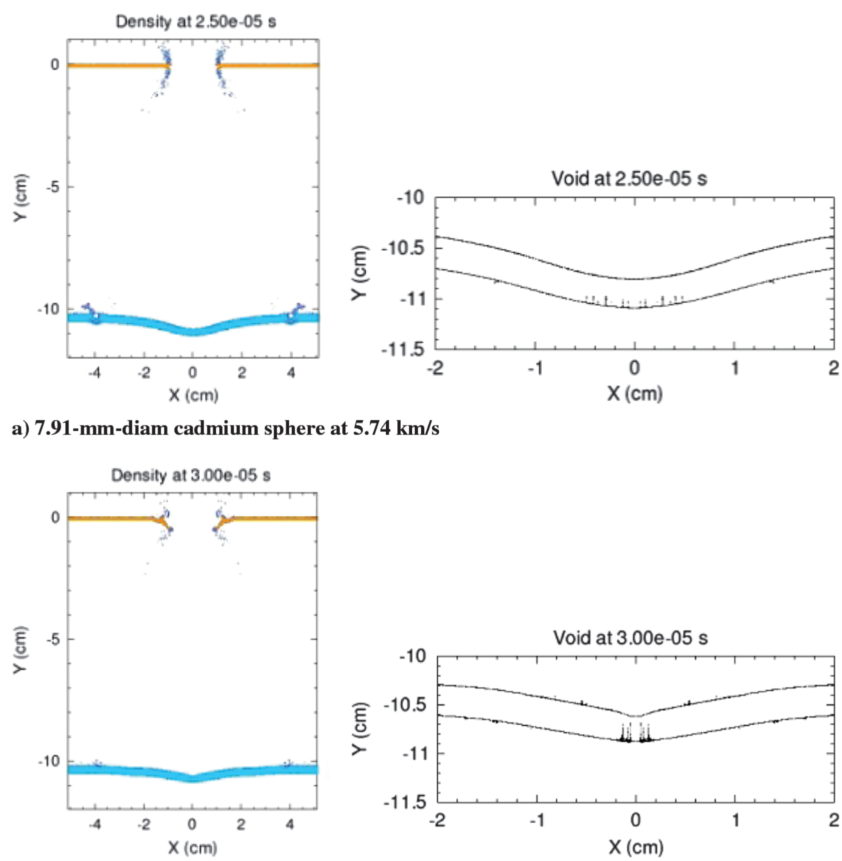

a) 7.91-mm-diam cadmium sphere at 5.74 km/s

b) 6.37-mm-diam cadmium sphere at 4.85 km/s

Fig. 12 Results from simulation of HVI tests performed with a Cadmium-based two-wall configuration [14].

sensitive to this change in dust material and predict less damage with the less dense dust material as expected.

A second set of computations, in which the solid Kapton bumper was replaced by a layered and spaced arrangement, was performed to verify the computational capability for modeling bumpers that are more representative of actual MLI blankets. The MLI was represented by 21 Kapton layers (one 80 μm outermost layer, nineteen 25 μm layers, and one 80 μm innermost layer) with 420-μm-thick spacing between adjacent layers. This stackup was developed by scaling an actual blanket by ~3× to obtain a total thickness of 0.0635 cm. These computations, performed for 20 and 80 km/s HVI, indicated that layering and introduction of spaces result in loss of shielding capacity as expected. Reducing the interlayer spacing to 210 μm was found to provide better shielding performance than obtained with 420 μm.

In addition to the verification of CTH's capability for performing SPP-relevant two-wall Whipple shield damage computations with the scaled-up configuration described in Fig. 7, comparison of

Downloaded by VIRGINIA TECHNICAL UNIVERSITY on March 18, 2015 | http://arc.aiaa.org | DOI: 10.2514/1.A33101

Downloaded by VIRGINIA TECHNICAL UNIVERSITY on March 18, 2015 | http://arc.aiaa.org | DOI: 10.2514/1.A33101

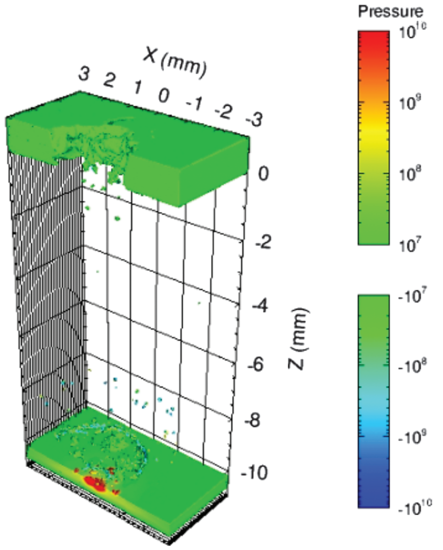

Fig. 13 Three-dimensional analysis of a two-wall Whipple shield with a 0.0127-cm-thick Kapton bumper, 1.0 cm standoff, and 0.0508-cm-thick titanium alloy Ti-6Al-4V rear wall, and fused silica dust.

simulations with the most relevant test data that could be obtained was performed. This effort resulted in three sets of validation analyses, namely, rear wall damage prediction under conditions of HVI by a vapor cloud (as opposed to a particulate/debris cloud), critical particle diameter prediction in a two-wall Whipple shield with a Kapton bumper, and critical particle diameter prediction for the case of MLI laid on top of a rear wall without a standoff.

For purposes of validating the 2-D CTH hydrocode computations of two-wall Whipple shields in the vaporization regime, the data involving cadmium projectiles, cadmium bumpers, and aluminum alloy rear walls developed by Schmidt et al. [14] were found to be most appropriate following an exhaustive review of the open literature. Specifically, test nos. 4-1407, 4-1410, 4-1419, and 4-1421 were simulated to evaluate CTH's capability for accurately modeling the transition from no failure to failure of a two-wall configuration in which a hot vapor blast develops after the interaction of the projectile and the bumper. Adaptive mesh refinement with square cells as small as 12.5×12.5 μm was used for these calculations. Tabular equations of state were used for cadmium and aluminum [22]. Johnson–Cook strength and failure models, along with spall strength values were used for the aluminum alloy rear wall [21,22]. The Whipple shield configuration consisted of a 0.127-cm-thick cadmium bumper, 10.2 cm standoff, and 0.318-cm-thick aluminum alloy 2219-T87 rear wall, and cadmium particles. Figure 12 shows results for the two cases in which the rear wall showed failure. In general, the predictions of rear wall failure were in very good agreement with the test results. The prediction for test no. 4-1421 showed material clustering along the symmetry axis, but this was for the lowest projectile mass and velocity case; the rear wall in the simulation of test no. 4-1419, which used a heavier and faster projectile, did not fail. Also, the relatively small computed rear wall deformation was consistent with the experimental result. It may be noted that the computations indicate a bending failure mode as opposed to planar-shock-induced spall development parallel to the wall free surfaces seen in Figs. 7–9.

As a means of validating the predictive capability for critical particle diameter in an SPP-relevant case, a configuration consisting of a 0.127-mm-thick solid Kapton bumper, 10 mm standoff, and 0.508-mm-thick titanium alloy Ti-6Al-4V rear wall was analyzed using 3-D CTH computations (Fig. 13) because of test data available for this specific configuration [24]. This configuration has a strong resemblance to an actual spacecraft configuration, which would have an MLI blanket with alternating microthin Kapton layers and polymeric netting instead of a pure Kapton monolith. Consistent with the data, the critical fused silica ($2.2\ \mathrm{g/cm^3}$) particle diameter for causing detached spall at $7\ \mathrm{km/s}$ is computed to be 700 μm (Fig. 14). The 0.0127-cm-thick ($0.018\ \mathrm{g/cm^2}$) Kapton bumper was modeled either with 25.4-μm-thick layers without any spacing between these layers (a and b), or as 13 Kapton layers (25 μm outermost, 11 7 μm, 25 μm innermost) with 140-μm-thick spacing between adjacent layers.

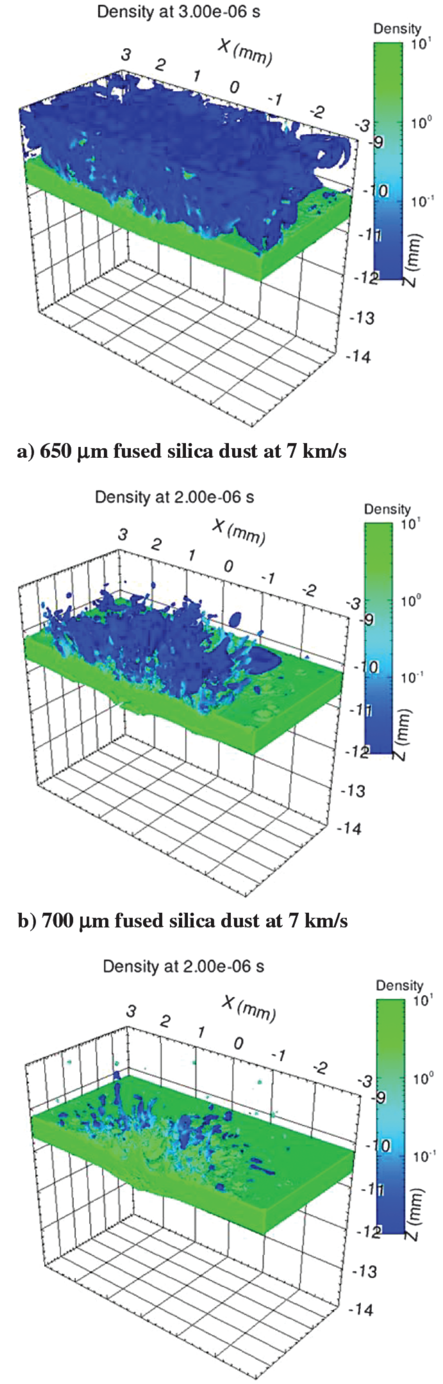

a) 650 μm fused silica dust at 7 km/s

b) 700 μm fused silica dust at 7 km/s

c) 650 μm fused silica dust at 7 km/s, 20 Kapton layers with standard spacing

Fig. 14 Damage in the rear wall of the configuration described in Fig. 13.

Three-dimensional computations were used for this problem to avoid the previously mentioned clustering of particulate material along the symmetry axis with 2-D (axisymmetric) grids (Figs. 8a and 8b). In general, all SPP computations at lower impact speeds were performed with a 3-D grid for this reason. The 3-D computational capability, including the level of grid refinement used (adaptive mesh refinement with 31.25 μm grid resolution), was additionally and separately verified by comparing the predicted critical particle diameters and rear wall damage (incipient spall) obtained from the already-verified 2-D analyses at higher SPP impact speeds (30–150 $\mathrm{km/s}$). Figure 15 shows representative comparisons and the good level of agreement between 3- and 2-D damage predictions.

Downloaded by VIRGINIA TECHNICAL UNIVERSITY on March 18, 2015 | http://arc.aiaa.org | DOI: 10.2514/1.A33101

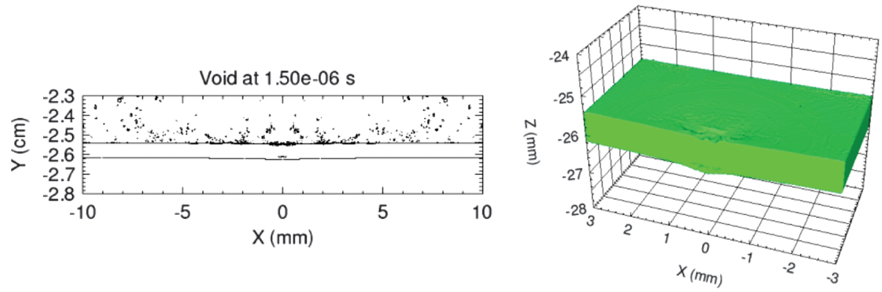

a) 610 μm dust at 30 km/s

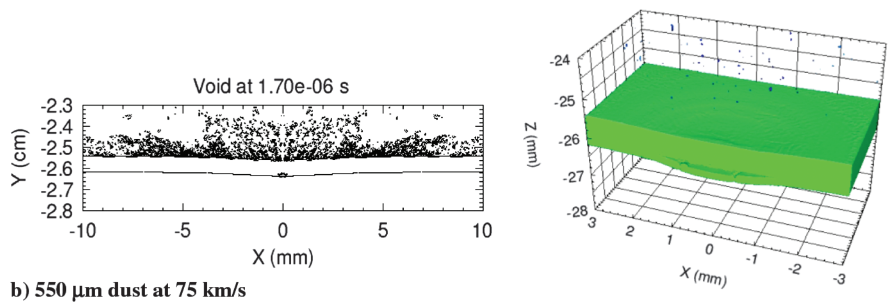

b) 550 μm dust at 75 km/s

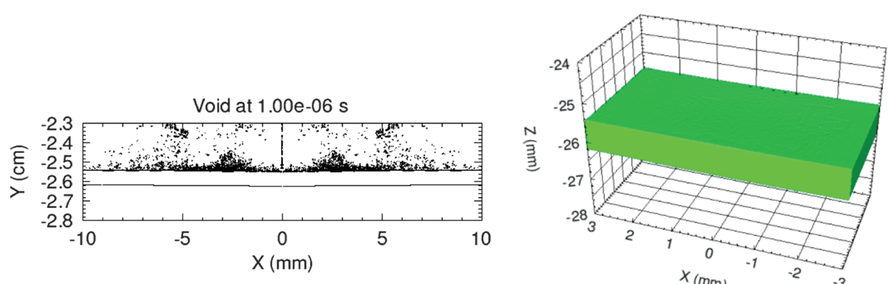

c) 450 μm dust at 150 km/s

Fig. 15 Verification of the 3-D computational capability.

To obtain some assessment of uncertainty involved with representing an actual MLI blanket by a series of equally spaced microthin Kapton layers without any netting, a case in which a blanket was placed on top of a rear wall (zero standoff) was analyzed (Fig. 14). The 0.0127-cm-thick (0.018 $\mathrm{g/cm^2}$) Kapton bumper was modeled either with 35.4-μm-thick layers without any spacing between these layers (a and b), or as 13 Kapton layers (25 μm outermost, 11 7-μm inner space, 25 μm innermost) with 140-μm-thick spacing between adjacent layers. In lieu of directly obtained test data, the existing BLE for this configuration was used [1]. The accuracy of the BLE for this configuration is believed to be similar to that for monolithic metallic shields. One analysis considered a particle that is sufficient to induce failure in the rear wall. The computation for this case (adaptive mesh refinement with 31.25 μm grid resolution) showed no damage in the rear wall, confirming the protective effect of the MLI. A second analysis determined that the critical particle diameter for causing incipient spall in the rear wall is 400 μm; the diameter predicted by the BLE for this case is 417 μm (Fig. 16).

Based on all of the foregoing verification and validation computations performed, a basis of confidence in the computational capability for modeling the shielding capability of MLI against dust HVI was established.

VI. Dust HVI Shielding Capability of MLI

To be able to define the risk to SPP spacecraft surfaces that will be covered with MLI and specify the related design trade space, baseline designs are defined for different areas of the spacecraft for evaluation. For the present purpose, the baseline design adopted for the SPP cooling system, consisting of a 0.05 $\mathrm{g/cm^2}$ (nominal) MLI bumper, 2.54 cm standoff, and a 0.0762-cm-thick titanium alloy Ti-6Al-4V rear wall, is described.

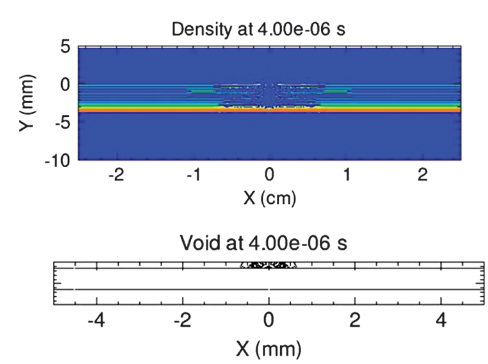

a) Particle diameter slightly larger than the critical particle for the wall alone

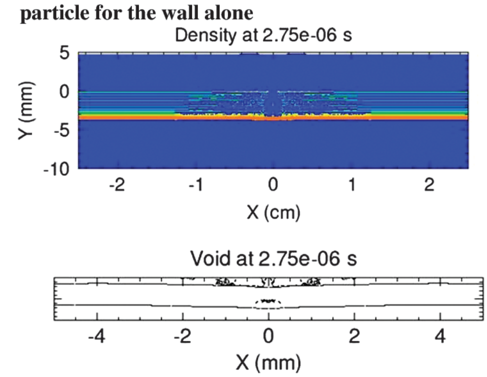

b) Particle diameter that just causes incipient spall

Fig. 16 Results from simulation of HVI tests with MLI lying placed on Titanium.

Downloaded by VIRGINIA TECHNICAL UNIVERSITY on March 18, 2015 | http://arc.aiaa.org | DOI: 10.2514/1.A33101

The baseline 0.05 $\mathrm{g/cm^2}$ (nominal) MLI is represented by 20 Kapton layers (one 25 μm outermost layer, eighteen 7-μm inner layers, and one 25 μm innermost layer) with 140 μm-thick spacing between adjacent layers. This stackup of Kapton layers gives an areal density of 0.025 $\mathrm{g/cm^2}$ in actuality. The remainder of the areal density, which would be from the 140 μm-thick polymeric netting layers, is neglected in the modeling. This reduced representation of MLI is believed to provide conservative estimates of MLI bumper shielding capability while permitting 2-D computations, both of which are desirable. Including the netting and its geometry would require 3-D modeling, currently unavailable material models, and bring in significant additional complexity through consideration of different netting overlays and dust entry locations relative to netting material locations.

As stated previously, the ultimate goal of this effort is to develop a BLE for generalizing a set of particular results and quantitatively specifying design requirements for SPP Whipple shields with MLI bumpers. Although blanket areal density can be accounted for as described earlier, and standoff and rear wall thickness and material properties can be accounted for through parametric computations, the spacing between the layers of an MLI blanket is generally not controlled. To evaluate MLI layer spacing as a design parameter in a BLE, computations were performed at two representative SPP impact speeds (30 and 150 km/s) in which the interlayer spacing was set to a value that is believed to be a reasonable upper bound (i.e., 320 μm). This gives a total blanket thickness of about 0.635 cm. These computations, compared with results for the baseline MLI spacing, showed that shielding performance is slightly reduced with the larger MLI spacing at 30 km/s, and that shielding performance is slightly enhanced with the larger MLI spacing at 150 km/s. At 30 km/s, the incipient spall in the rear wall was slightly more developed but the difference was not great enough to change the critical particle diameter (610 μm) within the desired level of accuracy (i.e., ± 20 μm). Similarly, at 150 km/s, the critical particle diameter (500 μm) was not affected by the MLI spacing within the desired accuracy, although in this case, the rear wall incipient spall was less developed with the greater spacing.

From a mechanistic standpoint, these results show that, at relatively low SPP impact speeds, such as 30 km/s, for which the expected dust size is somewhat larger, the response of the MLI layers may be more similar to that of an undersized bumper system [1]. However, at relatively high SPP impact speeds, such as 150 km/s, for which the expected SPP dust size is correspondingly smaller, the MLI layers seem to respond like a multishock shield [1]. The implication is that the loss of shielding performance with increased MLI layer spacing and dust impact speed may be bounded.

Extending the preliminary finding of a small effect of layer spacing on critical particle size to a broader assumption (i.e., MLI layer spacing does not affect the critical particle diameter in the range of speeds and blanket configurations most relevant to SPP) and considering that MLI areal density is generally increased by adding 7-μm-thick Kapton layers, the following simplified approach becomes possible for accounting for blanket areal density and number of layers as BLE design parameters:

1) Define critical particle sizes at relevant SPP velocities (e.g., 30, 75, and 150 km/s) for a given configuration (e.g., SPP baseline).

2) Obtain change in critical particle size with number of layers/areal density for specifying protection levels needed or achieved for other size-critical particles.

To account for the non-MLI Whipple shield design parameters, the existing two-wall Whipple shield BLE [1] can be evaluated and spot checked with select computations, as stated previously.

Figure 17 shows critical fused silica dust diameters for the SPP baseline configuration in the 30–150 km/s range. Adaptive mesh refinement with square cells as small as 7.5×7.5 μm was used for these calculations. Johnson–Cook strength and failure models, along with spall strength values were used for the titanium alloy rear wall [21,22]. The data differ from existing BLEs obtained by representing the MLI blanket as an aluminum alloy or Kapton monolithic bumper, which are also shown for comparison. Open symbols denote pass and closed symbols denote fail. Data differs from existing BLEs obtained by representing the MLI blanket as an aluminum alloy or Kapton monolithic bumper, which are also shown for comparison in Fig. 17. The reduction in critical particle diameter in the 30–150 km/s range is modest, indicating that the risk to the spacecraft from ultra-high-speed impacts is not as great as might have been expected by extrapolating existing monolith-based BLEs into speed regimes beyond those used to derive them. At speeds less than 7 km/s, the existing aluminum bumper BLE is indicated to be strongly nonconservative. At 7 km/s, the critical diameter is between 850 and 950 μm. Ground HVI testing with a configuration [0.05 $\mathrm{g/cm^2}$ (actual) MLI bumper, 2.54 cm standoff, and a 0.1016-cm-thick titanium alloy Ti-6Al-4V rear wall] that closely resembles the SPP baseline, performed after the computations, indicates that the critical soda lime glass (2.5 $\mathrm{g/cm^3}$) diameter is between 1000 and 1100 μm. This is consistent with the prediction for the SPP baseline configuration analyzed, in which the rear wall was slightly thinner (0.0762 cm). Additionally, a 3-D computation of the ground HVI test, in which the MLI netting is ignored, also indicates rear wall failure from a 7 km/s HVI of a 1100-μm-diam fused silica particle.

With a view toward generalizing these results to other values of bumper areal density, standoff, and rear wall thickness, comparisons are made with existing BLEs for monolithic bumpers. The existing BLE with an aluminum monolithic bumper with the same areal density as the MLI is arguably in adequate agreement with the computed results in the 30–150 km/s range, but it is nonconservative by a factor of $\sim 2\times$ at 7 km/s. The existing BLE with an equivalent Kapton monolithic bumper is found to be in good agreement with test data at 7 km/s, but conservative by a factor of $\sim 2\times$ in the 30–150 km/s range. These comparisons show that the actual BLE

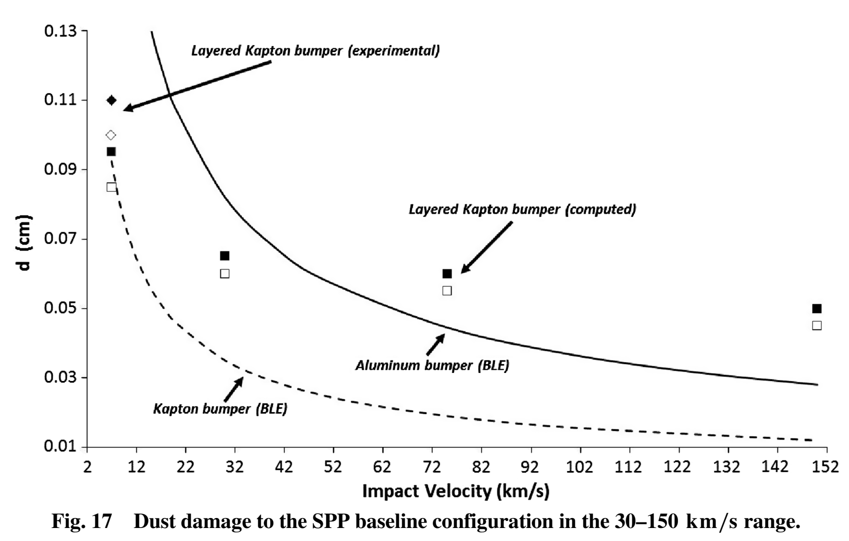

Fig. 17 Dust damage to the SPP baseline configuration in the 30–150 km/s range.

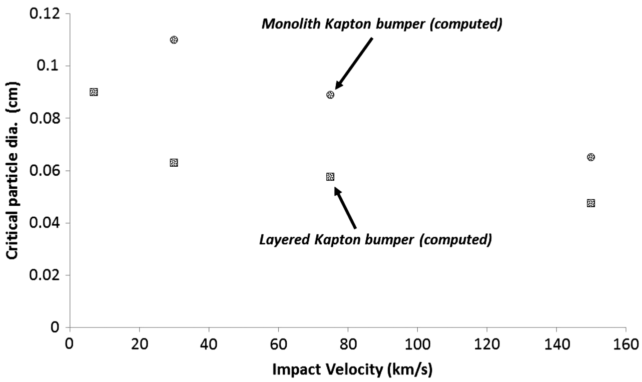

Fig. 18 Critical dust diameters for the SPP baseline configuration in the 30–150 km/s range.

Downloaded by VIRGINIA TECHNICAL UNIVERSITY on March 18, 2015 | http://arc.aiaa.org | DOI: 10.2514/1.A33101

for a blanket does not follow a two-third power dependence on the impact velocity, as obtained by energy scaling for impact cratering and generally also assumed for Whipple shield rear wall failure without any specific rationale. Figure 18, which compares computed BLE data obtained with the baseline MLI bumper and equivalent monolithic Kapton bumper, shows that the BLE would be steeper with a monolithic bumper; more so, the BLE for an MLI bumper would be relatively flat, particularly in the 30–150 km/s HVI range. From Fig. 10, it can be expected that the protection curve with an aluminum monolith bumper is even steeper. Data shown for layered Kapton bumper is the average of the points shown in Fig. 17.

Some analysis has also been performed to assess the effect of spacing between the Kapton layers (140 versus 320 μm) in a blanket on critical particle size in the 30–150 km/s HVI range. Little change in the critical particle size is found, suggesting that the response of the blanket layers to high-velocity IDP may be similar to that of multishock shields. Understanding the physics underlying the changing velocity dependence of Whipple shield rear wall damage as functions of bumper density and layering would require more fundamental analysis of specific dust breakup mechanisms and debris/vapor cloud characteristics.

VII. Conclusions

The Solar Probe Plus spacecraft is expected to encounter an interplanetary dust environment, which requires consideration of unprecedented impact speeds (i.e., up to 300 km/s) during its six to seven year mission. The traditional ground hypervelocity impact testing-based approach up to $\sim$10 km/s is inadequate for specifying spacecraft shielding and making associated risk assessments. A multiphysics computations-based methodology that combines design considerations with rigorous impact shock physics analyses, high-rate material thermodynamic and strength response models, shock hydrocode computations, and new and available test data has been practiced at the Johns Hopkins Applied Physics Laboratory to obtain the necessary information. This paper presents the effort specific to multilayer insulation/blanket shielded portions of the spacecraft and presents the essential elements of a new ballistic limit equation for this class of Whipple shield configurations.

The development of the ballistic limit equation in the 7–150 km/s hypervelocity impact range for representative two-wall Whipple shields, in which spacecraft multilayer insulation is the bumper material impacted by fused silica dust and normal (nonoblique) impacts, is achieved by combining: 1) test data at $\sim$7 km/s for a two-wall shield in which the bumper is a blanket or made with Kapton film only, 2) validated and verified two- and three-dimensional hydrocode computations of critical particle diameters, and 3) existing ballistic limit equations developed for two-wall Whipple shields with solid aluminum and Kapton monolithic bumpers, but applied in terms of the bumper areal density rather than thickness.

In the 30–150 km/s hypervelocity impact range, a Whipple shield that represents a baseline Solar Probe Plus configuration is adopted for three-dimensional analysis: 0.0176-cm-thick Kapton bumper (monolithic and layered), 2.54 cm standoff, and 0.0762-cm-thick titanium alloy Ti-6Al-4V rear wall. With a solid Kapton bumper, the critical particle diameter for incipient spall, which is chosen to be the failure criterion for Solar Probe Plus, is found to be in the $\sim$650–1100 μm range, with the largest and the smallest sizes corresponding to 30 and 150 km/s, respectively. When the bumper is layered in a manner similar to that found in actual blankets (140 μm spacing), the critical particle diameter is indicated to be in the $\sim$450–600 μm range.

The broad, thorough, and successful verification and validation of the numerics and physics of this complex problem, and the successful capacity to predict Whipple shield performance at ground hypervelocity impact speeds, suggest that computationally derived hypervelocity impact shielding data that are coequal to experimentally derived data in terms of quality and reliability are possible to obtain.

Acknowledgments

This work was sponsored by NASA Goddard Space Flight Center Living with a Star Program Office. Mark Goans is the Deputy Program Manager for Johns Hopkins Applied Physics Laboratory programs. The authors wish to thank team members P. K. Swaminathan, Robert Brown, and Cesar Carrasco for helpful discussions.

References

[1] Christiansen, E. L., Arnold, J., Davis, A., Hyde, J., Lear, D., Liou, J.-C., Lyons, F., Prior, T., Ratliff, M., Ryan, S., Giovane, F., Corsaro, R., and Studor, G., "Handbook for Designing MMOD Protection," NASA TM-2009-214785, June 2009.

[2] Piekutowski, A. J., Poormon, K. L., Christiansen, E. L., and Davis, B. L., "Performance of Whipple Shields at Impact Velocities Above 9 km/s," *International Journal of Impact Engineering*, Vol. 38, No. 6, 2011, pp. 495–503.
doi:10.1016/j.ijimpeng.2010.10.021

[3] Christiansen, E. L., and Kerr, J. H., "Ballistic Limit Equations for Spacecraft Shielding," *International Journal of Impact Engineering*, Vol. 26, Nos. 1–10, 2001, pp. 93–104.
doi:10.1016/S0734-743X(01)00070-7

[4] Chhabildas, L. C., Hertel, E. S., and Hill, S. A., "Hypervelocity Impact Tests and Simulations of Single Whipple Bumper Shield Concepts at 10 km/s," *International Journal of Impact Engineering*, Vol. 14, Nos. 1–4, 1993, pp. 133–144.
doi:10.1016/0734-743X(93)90015-Y

[5] Mehoke, D. S., Swaminathan, P. K., Carrasco, C. J., Brown, R. C., Kerley, G. I., and Iyer, K. A., "Review of the Solar Probe Dust Protection Approach," *Proceedings of the IEEE Aerospace Conference*, IEEE Publ., Piscataway, NJ, 2012, pp. 1–13.
doi:10.1109/AERO.2012.6187076

[6] Iyer, K. A., Mehoke, D. S., Brown, R. C., Swaminathan, P. K., Carrasco, C. J., and Batra, R. C., "Use of Hydrocode Modeling to Develop Advanced MMOD Shielding Designs," *Proceedings of the IEEE Aerospace Conference*, IEEE Publ., Piscataway, NJ, 2012, pp. 1–13.
doi:10.1109/AERO.2012.6187075

[7] Whipple, F. L., "Meteorites and Space Travel," *Astronomical Journal*, Vol. 52, 1947, p. 131.
doi:10.1086/106009

[8] Maiden, C. J., McMillan, A. R., and Sennett, R. E., III, "Thin Sheet Impact," NASA CR-295, Sept. 1965.

[9] Madden, R., "Ballistic Limit of Double-Walled Meteoroid Bumper Systems," NASA TN-D-3916, April 1967.

[10] Nysmith, C. R., "Penetration Resistance of Double-Sheet Structures at Velocities to 8.8 km/s," NASA TN-D-4568, May 1968.

[11] Richardson, A. J., "Theoretical Penetration Mechanics of Multisheet Structures Based on Discrete Debris Particle Modeling," *Journal of Spacecraft and Rockets*, Vol. 7, No. 4, 1970, pp. 486–489.
doi:10.2514/3.29972

[12] Piekutowski, A. J., "Formation and Description of Debris Clouds Produced by Hypervelocity Impact," NASA CR-4707, Feb. 1996.

[13] Hopkins, A. K., Lee, T. W., and Swift, H.F., "Material Phase Transformation Effects upon Performance of Spaced Bumper Systems," *Journal of Spacecraft and Rockets*, Vol. 9, No. 5, 1972, pp. 342–345.
doi:10.2514/3.61684

[14] Schmidt, R. M., Housen, K. R., Piekutowski, A. J., and Poormon, K. L., "Cadmium Simulation of Orbital-Debris Shield Performance to Scaled Velocities of 18 km/s," *Journal of Spacecraft and Rockets*, Vol. 31,

No. 5, 1994, pp. 866–877.
doi:10.2514/3.26525

[15] Schonberg, W. P., and Peck, J. A., "Multi-Wall Structural Response to Hypervelocity Impact: Numerical Predictions vs Experimental Results," *International Journal of Impact Engineering*, Vol. 13, No. 1, 1993, pp. 117–132.
doi:10.1016/0734-743X(93)90111-J

[16] Hertel, E. S., McIntosh, R. L., and Patterson, B. C., "Comparison of Phase Change Phenomena in CTH with Experimental Data," *International Journal of Impact Engineering*, Vol. 17, Nos. 1–3, 1995, pp. 399–408.
doi:10.1016/0734-743X(95)99865-O

[17] Taylor, E. A., "Simulation of Hollow Shaped Charge Jet Impacts onto Aluminum Whipple Bumpers at 11 km/s," *International Journal of Impact Engineering*, Vol. 26, Nos. 1–10, 2001, pp. 773–784.
doi:10.1016/S0734-743X(01)00129-4

[18] Thoma, K., Riedel, W., Schafer, F., and Hiermaier, S., "Status and Perspectives in Protective Design," *Space Debris*, Vol. 2, No. 4, 2000, pp. 201–224.
doi:10.1023/B:SDEB.0000029884.04355.9a

[19] McGlaun, J. L., Thompson, S. L., and Elrick, M. G., "CTH: A Three-Dimensional Shock Wave Physics Code," *International Journal of Impact Engineering*, Vol. 10, Nos. 1–4, 1990, pp. 351–360.
doi:10.1016/0734-743X(90)90071-3

[20] Stadermann, F. J., Heiss, C. H., and Reichling, M., "Evaluation of Impact Craters on Solar Cell Samples and Thermal MLI Blankets," *Advances in Space Research*, Vol. 20, No. 8, 1997, pp. 1517–1521.
doi:10.1016/S0273-1177(97)00429-8

[21] Iyer, K. A., Poormon, K. L., Deacon, R. M., Mehoke, D. S., Swaminathan, P. K., and Brown, R. C., "Hypervelocity Impact Response of Ti-6Al-4V and Commercially Pure Titanium," *Procedia Engineering*, Vol. 58, 2013, pp. 127–137.
doi:10.1016/j.proeng.2013.05.016

[22] Crawford, D. A., Brundage, A. L., Harstad, E. L., Ruggirello, K., Schmitt, R. G., Schumacher, S. C., and Simmons, J. S., "CTH User's Manual and Input Instructions," Sandia National Lab., Albuquerque, NM, 2012.

[23] Kerley, G. I., "Equation of State and Constitutive Models for Numerical Simulations of Dust Impacts on the Solar Probe," Johns Hopkins Applied Physics Lab., Rept. on Contract No. 949182, Laurel, MD, 2009.

[24] Davis, M. L., Kichak, R. A., Christiansen, E. L., Ratliff, M., Cooke, W. J., Suggs, R. M., Womack, J. M., Colangelo, T., Galbraith, J., and Robinson, J. R., "James Webb Space Telescope Integrated Science Instrument Module Electrical Cable Protection," NASA TM-2009-215907, Aug. 2009.

T. Minton
Associate Editor

Downloaded by VIRGINIA TECHNICAL UNIVERSITY on March 18, 2015 | http://arc.aiaa.org | DOI: 10.2514/1.A33101